

Cold Molecular Gas and Free-Free Emission from Hot, Dust-Obscured Galaxies at $z \sim 3$

J.I. Penney,^{1*} A. W. Blain,¹ R. J. Assef,² T. Diaz-Santos,^{2,3,4} J. González-López,^{2,5}
C. -W. Tsai,⁶ M. Aravena,² P. R. M. Eisenhardt,⁷ S. F. Jones,⁸ H. D. Jun,⁹
M. Kim,¹⁰ D. Stern,⁷ J. Wu⁶

¹Department of Physics and Astronomy, University of Leicester, University Road, Leicester, LE1 7RH, UK

²Núcleo de Astronomía de la Facultad de Ingeniería y Ciencias, Universidad Diego Portales, Av. Ejército Libertador 441, Santiago, Chile

³Chinese Academy of Sciences South America Center for Astronomy (CASSACA), National Astronomical Observatories, CAS, Beijing 100101, China

⁴Institute of Astrophysics, Foundation for Research and Technology Hellas, Heraklion, GR-70013, Greece

⁵Las Campanas Observatory, Carnegie Institution of Washington, Casilla 601, La Serena, Chile

⁶National Astronomical Observatories, Chinese Academy of Sciences, 20A Datun Road, Chaoyang District, Beijing, 100012, China

⁷Jet Propulsion Laboratory, California Institute of Technology, 4800 Oak Grove Drive, CA 91109, USA

⁸Department of Space, Earth, and Environment, Chalmers University of Technology, Onsala Space Observatory, SE-43992, Onsala, Sweden

⁹School of Physics, Korea Institute for Advanced Study, 85 Hoegiro, Dongdaemun-gu, Seoul 02455, Korea

¹⁰Department of Astronomy and Atmospheric Sciences, Kyungpook National University, Daegu 702-701, Korea

Accepted XXX. Received YYY; in original form ZZZ

ABSTRACT

We report on observations of redshifted CO(1–0) line emission and observed-frame ~ 30 GHz radio continuum emission from five ultra-luminous, mid-IR selected hot, Dust-Obscured Galaxies (Hot DOGs) at $z \gtrsim 3$ using the Karl G. Jansky Very Large Array. We detect CO(1–0) line emission in all five Hot DOGs, with one of them at high signal to noise. We analyse FIR-radio spectral energy distributions, including dust, free-free and synchrotron emission for the galaxies. We find that most of the 115 GHz rest-frame continuum is mostly due to synchrotron or free-free emission, with only a potentially small contribution from thermal emission. We see a deficit in the rest-frame 115 GHz continuum emission compared to dusty star-forming galaxies (DSFGs) and sub-millimetre galaxies (SMGs) at high redshift, suggesting that Hot DOGs do not have similar cold gas reserves compared with star-forming galaxies. One target, W2305-0039, is detected in the FIRST 1.4 GHz survey, and is likely to possess compact radio jets. We compare to the FIR-radio correlation, and find that at least half of the Hot DOGs in our sample are radio-quiet with respect to normal galaxies. These findings suggest that Hot DOGs have comparably less cold molecular gas than star-forming galaxies at lower, $z \sim 2$ redshifts, and are dominated by powerful, yet *radio-quiet* AGN.

Key words: radio lines: galaxies – galaxies: active – galaxies: evolution

1 INTRODUCTION

Galaxy evolution models currently predict that the formation of most massive galaxies ($M_* \gtrsim 10^{12} M_\odot$) involve major mergers at high redshift (see [Conselice 2014](#), and references therein). This major-merger theory could be key to understanding how elliptical galaxies form ([Toomre 1977](#); [Barnes & Hernquist 1998](#); [Kormendy & Bender 2012](#)). Mergers cause large quantities of gas to be forced into the cen-

tral regions of the galaxies, with some accreting onto a central super-massive black hole (SMBH) ([Hopkins et al. 2008](#)). Mergers produce a burst of high-mass star formation as cold gas condenses in giant molecular clouds, with some expelled in winds ([Sanders et al. 1988](#); [Barnes & Hernquist 1992](#); [Schweizer & Seitzer 1998](#); [Faucher-Giguère & Quataert 2012](#)).

Radio observations are critical to understanding star formation in galaxies at high redshift, providing high resolution images and estimates of the amount and dynamics of cold star-forming gas within the host galaxy. Molecular

* E-mail: jip3@leicester.ac.uk

Table 1. Properties of the sample in this paper, showing the CO(1–0) position, redshift, major and minor axis of the synthesized beam in the VLA images, and the position angle of the synthesized beam. All targets are roughly the same size as the beam. Redshifts, discussed in Section 3, are based on optical and near-IR spectroscopy (Wu et al. 2012; Tsai et al. 2015), although W0126-0529 has an ambiguous redshift detection and the most recent redshift has been placed in parentheses (see Jun et al. 2020). Here, (*) shows an ALMA redshift identification from CO($J=6-5$) emission.

WISE Designation	RA (J2000)	DEC (J2000)	z	Major (arcsec)	Minor (arcsec)	PA (deg)
W0116–0505	01:16:01.49	-05:05:05.1	3.173	4.00	2.62	–30.96
W0126–0529	01:26:11.95	-05:29:09.1	2.937 (0.8301)	4.17	2.44	–36.48
W0410–0913	04:10:10.62	-09:13:05.8	3.630*	4.08	2.92	–9.59
W0831+0140	08:31:53.25	01:40:10.3	3.912	3.78	3.06	–2.69
W1322–0328	13:22:32.55	-03:28:42.7	3.043	3.37	2.52	6.28
W2305–0039	23:05:25.93	-00:39:25.3	3.106	3.61	2.64	–29.03

hydrogen (henceforth H_2) gas traces regions of future star formation, though with strongly forbidden transitions it can only be observed at high temperatures ($T > 100$ K). The second most abundant molecule in the universe however, ^{12}CO , is readily excited and more easily observed. The lowest ^{12}CO transition, $^{12}CO(J=1-0)$ (henceforth CO(1–0)), traces the coldest molecular gas (Omont 2007; Ivison et al. 2011; Bolatto et al. 2013). CO(1–0) transitions are fainter than the higher J -transitions (Bolatto et al. 2013), but should more accurately measure the molecular gas content in galaxies. By assuming ^{12}CO and H_2 are linked (Solomon et al. 1997; Tacconi et al. 2008; Bolatto et al. 2013), the mass of the H_2 regions can be estimated. Further, detection of the lowest CO(1–0) transitions can be used in tandem with higher transitions (e.g. $J=4-3$) to understand properties such as local density of gas, the star formation rate and temperature of the star-forming gas (e.g. Peñaloza et al. 2017). Thus, from CO(1–0) observations, we can understand the molecular gas content necessary to form stars in high redshift galaxies, potentially isolating star formation in the surrounding galaxy from high-redshift, powerful AGN.

Hot, Dust-Obscured Galaxies (Hot DOGs; Wu et al. 2012) are hyper-luminous infra-red (IR) galaxies (HyLIRGs¹) initially discovered using the *Wide-field IR Survey Explorer* (WISE; Wright et al. 2010) All-Sky Survey (Cutri et al. 2012) by selecting for bright detections in the W3 ($12\ \mu\text{m}$) and W4 ($22\ \mu\text{m}$) bands and faint or no detections in the W1 ($3.4\ \mu\text{m}$) and W2 ($4.6\ \mu\text{m}$) bands (Eisenhardt et al. 2012). Follow-up observations by Wu et al. (2012) to determine more complete spectral energy distributions (SEDs) suggest significantly higher fractions of hot dust ($\gtrsim 60$ K) than most dusty galaxies, with a peak in their SEDs at rest-frame $\sim 22\ \mu\text{m}$, and high IR luminosities ($> 10^{13} L_{\odot}$; Jones et al. 2014; Tsai et al. 2015).

Optical spectra typically reveal narrow AGN lines, explaining their high luminosities and dust temperatures (Tsai et al. 2015). Follow-up observations using the *Spitzer Space Telescope* (henceforth *Spitzer*; Werner et al. 2004) show mid-IR SEDs consistent with obscured AGN emission (Assef et al. 2015). $850\ \mu\text{m}$ SCUBA-2 observations (Jones et al. 2014) show these galaxies inhabit overdense

environments of sub-millimeter galaxies (SMGs; Blain et al. 2002), with number densities within $1.5'$ of the galaxies ~ 3 times higher than blank fields. Assef et al. (2015) used warm-*Spitzer* observations to show these galaxies reside in regions with elevated surface densities of IRAC colour-selected galaxies, consistent with the rich environments of radio-loud AGN. For instance, the Clusters around Radio-Loud AGN (CARLA; Wylezalek et al. 2013) survey found that 92% of the ~ 400 radio-loud AGN they observed with *Spitzer* are overdense compared to the field, with most (55%) overdense at the $\geq 2\sigma$ level on $1'$ radius scales. Given the similar overdensity for Hot DOGs compared with radio-loud galaxies in Wylezalek et al. (2013), it is of interest to understand the ~ 1.4 GHz radio properties of Hot DOGs and whether they are similar to radio-loud galaxies or to the overall AGN population.

The Karl G. Jansky Very Large Array (VLA; Perley et al. 2011) has full coverage between 1 and 50 GHz with its upgrade in 2011, and it can now make unprecedented radio observations over a large frequency range. Here, we present CO(1–0) and rest-frame 115.3 GHz continuum observations of a sample of six hyper-luminous Hot DOGs from Tsai et al. (2015) using the lowest resolution and most sensitive configuration of the VLA (Table 1). These galaxies were selected for their high luminosities ($L_{\text{bol}} \geq 10^{14} L_{\odot}$). We use the VLA to obtain CO(1–0) luminosities and rest frame 115.3 GHz continuum fluxes of these galaxies to infer H_2 masses, as well as free-free and thermal activity of these highly obscured galaxies at the peak redshift of major mergers, which is before the peak redshift for starbursts and AGN activity (Hopkins et al. 2008).

Section 2 describes details of the observations, Section 3 discusses the main results of these observations and Section 4 uses archival data in conjunction with new radio observations to construct SEDs of the galaxies. Section 5 discusses these findings. Throughout, we assume a cosmology of $H_0 = 70\ \text{km s}^{-1} \text{Mpc}^{-1}$, $\Omega_m = 0.30$ and $\Omega_{\Lambda} = 0.70$.

2 OBSERVATIONS AND DATA REDUCTION

Observations of six sources (Table 1) were carried out in 1 – 2 hr blocks during generally excellent weather conditions between February and April 2017. The most compact baseline, D configuration, was used for the observations due to its greater sensitivity. Two observation blocks were used for each galaxy in our sample, except for W0126-0529, which had a single ~ 2 hr observation. The K-band

¹ Here, LIRGs, ULIRGs and HyLIRGs are characterized by a total IR luminosities of $10^{11} < L_{8-1000\ \mu\text{m}}/L_{\odot} < 10^{12}$, $10^{12} < L_{8-1000\ \mu\text{m}}/L_{\odot} < 10^{13}$ and $L_{8-1000\ \mu\text{m}}/L_{\odot} > 10^{13}$, respectively (Sanders & Mirabel 1996).

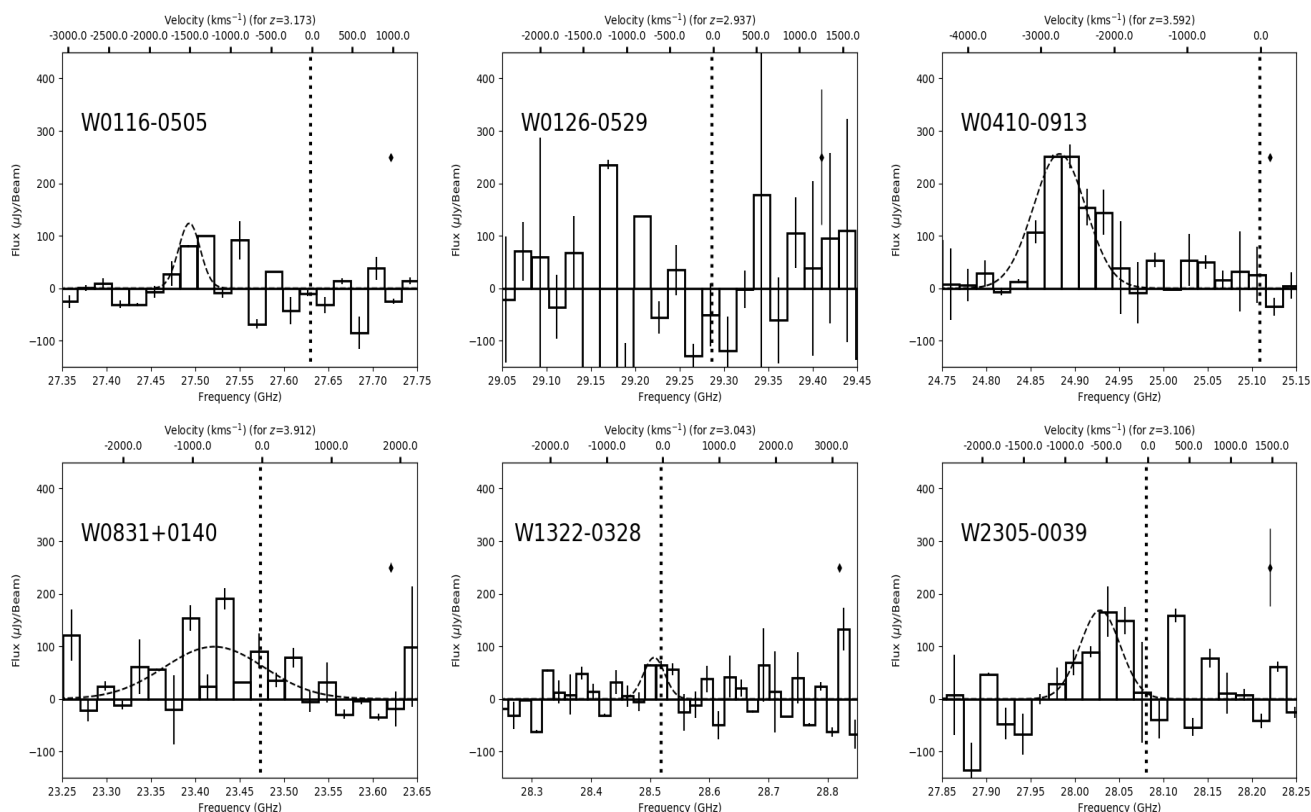


Figure 1. Continuum subtracted spectra of the six sources in our sample. A Gaussian has been added to illustrate the CO(1–0) line. An additional error bar in the upper right-hand corner has been included to show the average continuum level for each field. Dotted vertical lines indicate the expected CO(1–0) wavelength based on optical/IR redshifts (see Tsai et al. 2015). Frequency ranges have been chosen to highlight the line emission of the galaxies.

($\nu=18.0\text{--}26.5$ GHz) receiver was used for W0410-0913 and W0831+0140, and Ka-band ($\nu=26.5\text{--}40.0$ GHz) for W0116-0505, W0126-0529, W1322-0328 and W2305-0039. A single polarization was used, and the flux calibrators were 3C48 (for W0116-0505, W0126-0529 and W2305-0039), 3C138 (for W0410-0913 and W0831+0140), and 3C286 (for W1322-0328). The observations produced ~ 1 GHz bandwidth spectra centred on the expected CO(1–0) emission frequency ($\nu_{\text{rest}} = 115.3$ GHz; Morton & Noreau 1994) based on redshifts from optical/IR spectra presented in Wu et al. (2012) and Tsai et al. (2015).

Calibration and imaging were carried out using the Common Astronomy Software Application (CASA; McMullin et al. 2007a)². Calibrations were made using the pipeline³ for all fields except W1322-0328, in which a custom calibration method detailed in the online calibration cookbook⁴ was used for one of the observation blocks because of artefacts arising from a bad reference antenna using the pipeline. No additional calibrations were required following the pipeline calibrations.

The six fields were cleaned using CASA’s TCLEAN pack-

age. Initial dirty spectral maps were made to estimate the positions of the galaxies and the frequency of emission. Continuum subtraction was then carried out using the UVCONTSUB package. Cleaning and imaging of all fields was made using HOGBOM deconvolution, with BRIGGS weighting and ROBUST = 2.0 to produce a natural weighting. All spectral cubes were constructed using 6 MHz (50 km s^{-1}) resolution to boost the signal-to-noise ratio (SNR). Spectra were extracted using a single $0.05''$ pixel centred on the positions of the peak CO(1–0) emission, determined using CASA’s IMFIT routine, as shown in Table 1.

3 OBSERVATIONAL RESULTS

The spectra for the six targets in our sample are shown in Fig. 1. Errors are calculated from each individual channel of the spectra, and is $\sim 10\text{--}20\%$ of the peak flux for each frame. W0410-0913 has the strongest emission line, with a SNR of 4.21 at the peak and redshift of $z = 3.633 \pm 0.005$, (compared with an optical redshift of $z = 3.592 \pm 0.002$ from Wu et al. 2012). The CO(1–0) redshift matches the redshift from the CO($J=6\text{--}5$) line detection using ALMA (González-López et al. in prep.). This suggests that the gas associated with the lower, optical redshift could be emitted from outflows at $\sim 3000 \text{ km s}^{-1}$. This is expected, given work by Díaz-Santos et al. (2018), which saw blue-shifted lines from Ly α in another Hot DOG, W2246-0526.

² <https://casa.nrao.edu>

³ <https://science.nrao.edu/facilities/vla/data-processing/pipeline/scripted-pipeline>

⁴ https://casaguides.nrao.edu/index.php/TWHydraBand7_Imaging_4.3

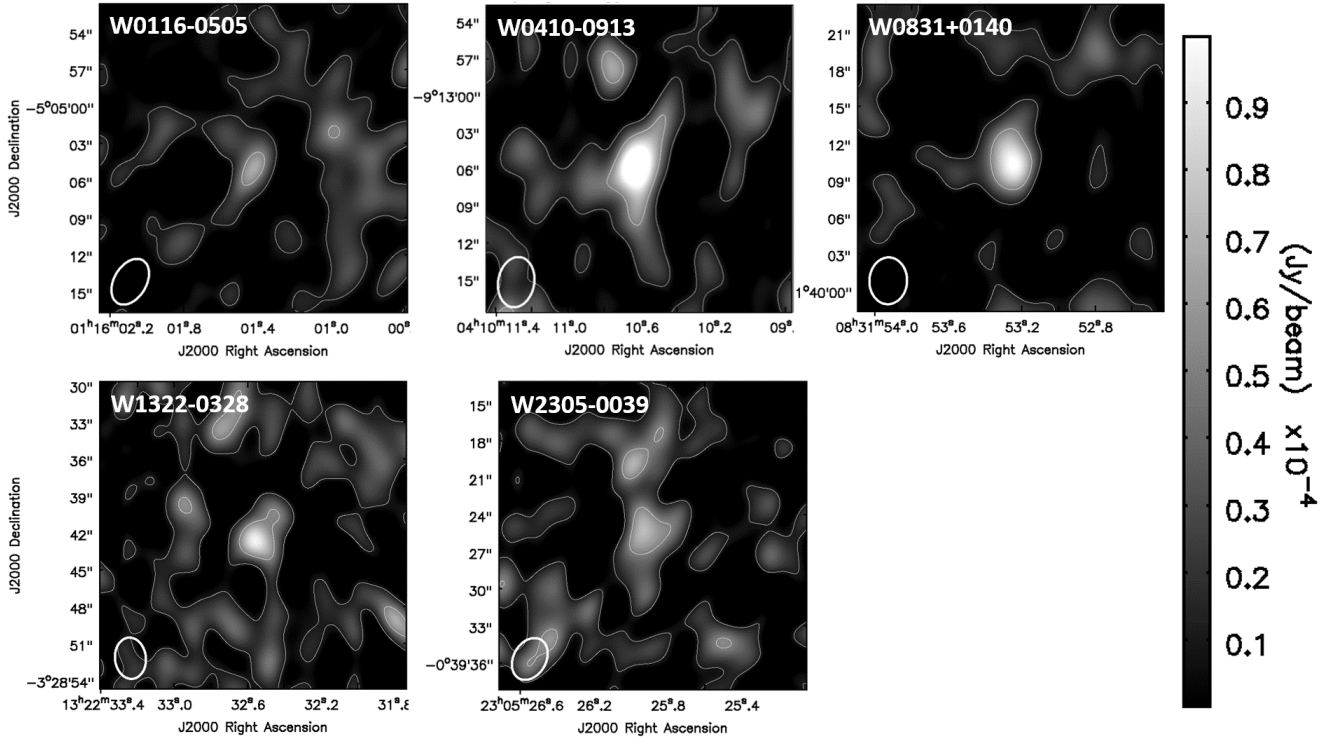


Figure 2. Emission centred images (moment=0) for W0116-0505, W0410-0913, W0831+0140, W1322-0328 and W2305-0039 with continuum subtraction. Contours show the $0.1 \mu\text{Jy}$, $0.5 \mu\text{Jy}$ and $1 \mu\text{Jy}$ levels. An ellipse in the bottom left-hand corner of each image illustrates the synthesized beam for each image.

The other galaxies in our sample show evidence of weak CO(1–0) emission, with the exception of W0126-0529, which has the least confident redshift identification in Tsai et al. (2015), based on a weak emission line assumed to be Ly α . Jun et al. (2020) determined a lower redshift for this galaxy using X-SHOOTER data: $z = 0.8301$. From our VLA observations, we confirm that there is no CO(1–0) emission at a redshift of $z = 2.937$. Based on these findings, the galaxy does not meet the luminosity selection criterion for the sample, and has been omitted from the rest of the discussion of the paper. All of the results for this object have been included in Appendix A. The emission line from W0116-0505 is at a lower frequency than expected, by $\delta\nu = 0.09$ GHz, a redshift of $z = 3.187 \pm 0.005$, compared to $z = 3.173 \pm 0.002$ in Wu et al. (2012). The velocity difference of $\sim 1400 \text{ km s}^{-1}$ suggests that the optically detected gas in W0116-0505 is also associated with out-flowing material. The CO(1–0) redshifts for W0831+0140, W1322-0328 and W2305-0039 agree with the optical/IR redshifts in Tsai et al. (2015), within $\delta\nu \sim 500 \text{ km s}^{-1}$. The full width at half-maximum (FWHM) of the fitted Gaussian for each of the galaxies is between $\sim 140\text{--}470 \text{ km s}^{-1}$ (see Table 2), much broader than the Milky Way CO(1–0) emission ($\lesssim 20 \text{ km s}^{-1}$; Sheth et al. 2008).

The images of the CO(1–0) emission are shown in Fig. 2 in the spectral window (henceforth *spw*) centred on the detected emission line and the entire *spw* centred on the emission line is used. All galaxies show line and continuum emission centred on the target. All fields have a $\text{SNR} \gtrsim 3$ (mean $\text{SNR} = 4.49$), showing that the positions of the emission lines are similar to the expected positions from previous observations of these galaxies, implying they are unlikely to

be significantly affected by background noise. Despite these relatively low SNRs, we can assume the VLA emission is attributed to these galaxies given the prior that these galaxies are detected at these positions at other wavelengths.

Using CASA’s IMMOMENTS, we imaged the velocity fields of the five Hot DOGs (moments= 1) to investigate any motion of molecular gas using the *spw* associated with the emission lines. We find no signs of rotational motion of the gas, as expected given the modest resolution and SNR of our observations. Unsurprisingly, there is no evidence for large-scale bulk motion of cold molecular gas around these galaxies on 20–50 kpc (3–6’’) scales. The cold molecular gas could have a velocity gradient in the Hot DOGs, as shown by the width of the CO(1–0) line in Fig. 1, suggesting that the cold molecular gas has not been evaporated by the emission of the central AGN. However, we are unable to detect the motion of the cold molecular gas given the current data. Greater spatial resolution and sensitivity are needed to understand whether there is any outflow of cold molecular CO gas responsible for the change in expected emission from W0116-0505.

We now compare our VLA observations with independent observations using ALMA (González-López et al. in prep.). These ALMA observations primarily looked at potential companion sources using higher *J*-components, looking at the warmer molecular gas in the environments of Hot DOGs. ALMA observations of W0116-0505, W0831+0140, W1322-0328 and W2305-0039 were taken as part of project 2017.1.00358.S, using ALMA’s Band-3 (2.6 – 3.6 mm) to image CO(*J*=4–3) emission. Additional observations were made for W0410-0913 using Band-5 (1.4 – 1.8 mm) to image

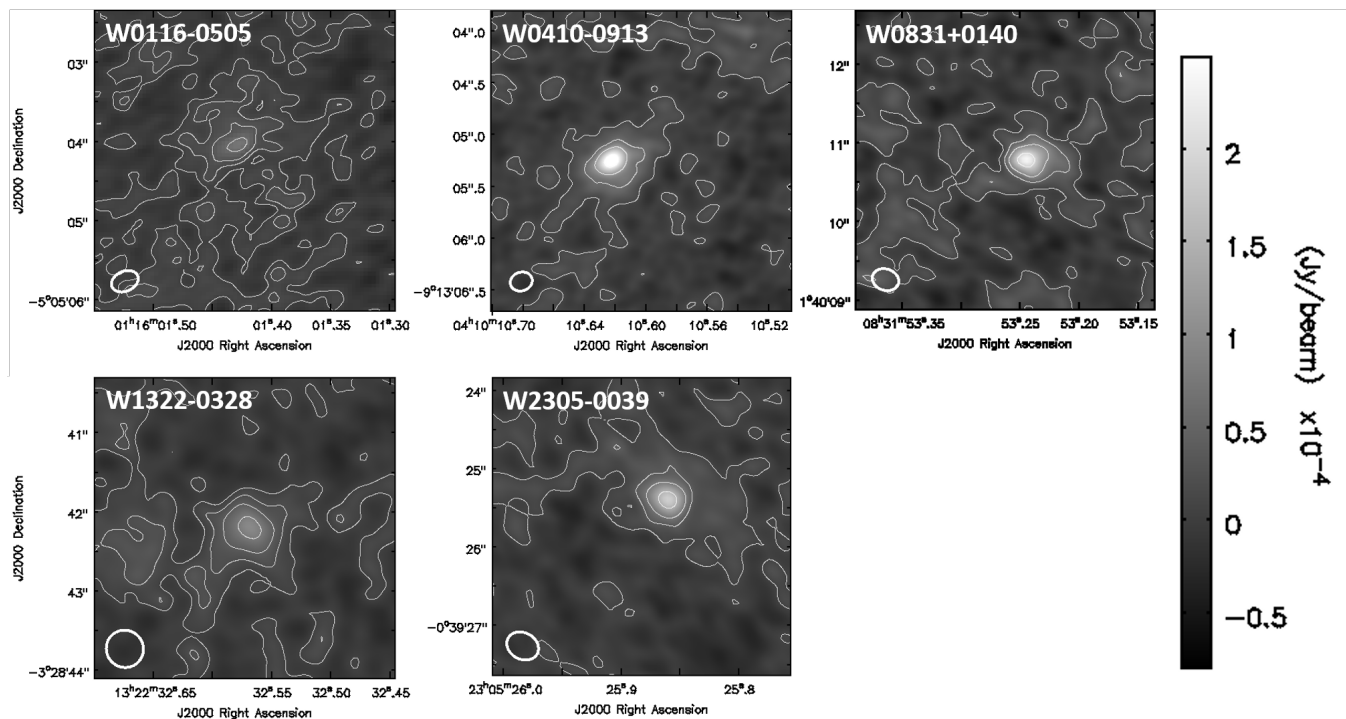


Figure 3. Continuum images of the five Hot DOGs in the sample observed using ALMA in Band-3 (2.6–3.6 mm) and Band-5 (1.4–1.8 mm) for W0410-0913. Contours show the $0.1\mu\text{Jy}$, $0.5\mu\text{Jy}$, $1\mu\text{Jy}$ and $2\mu\text{Jy}$ levels. An ellipse in the bottom left-hand corner of each image illustrates the synthesized beam for each image. A colour-bar has been provided to show the flux levels across the images.

CO($J=5-4$) emission as part of project 2017.1.00908.S. The data were processed with the ALMA calibration pipeline in CASA (McMullin et al. 2007b), using scripts provided by ALMA. The images and data cubes were created using the task TCLEAN with natural weighting. The continuum image was obtained using the multi-frequency synthesis (mfs) mode with all the line-free spw . Continuum emission was then subtracted from the visibilities using UVCONTSUB. All of the continuum images and data cubes were cleaned down to the 2σ level using auto-masking. The typical RMS value for the continuum maps was $9 - 15\mu\text{Jy beam}^{-1}$ with a beam size ranging from $0.2-0.5''$. Continuum measurements were carried out using the task IMFIT, and were checked using aperture photometry, which uncovered similar results. Fig. 3 shows the continuum maps for the ALMA observations.

From the VLA observations in Fig. 2, we see a potential companion to W2305-0039 within $\sim 5''$ of the Hot DOG (RA=23:05:26.00, DEC=-00:39:19.91) and is of interest due to the proximity to the target. Inspecting the VLA spectrum at the position of this additional source, we find a peak at a frequency corresponding to the same redshift of CO(1-0) emission as W2305-0039 ($L'_{\text{CO}(1-0)} = 0.88 \pm 0.50 \times 10^{10} \text{ K km s}^{-1} \text{ pc}^2$). Comparing with ALMA observations of warmer CO($J=4-3$) gas from González-López et al. (in prep.) at this position we find a lack of peak in the spectrum, suggesting that the companion is not composed of warmer CO gas. The W2305-0039 companion is likely to either be a site of additional cold molecular gas within the Hot DOG, or associated with the synchrotron emission seen

in the FIRST⁵ survey (see Section 5.1). We discuss the luminosity of these Hot DOGs with respect to observations of other galaxies in Section 3.1.

3.1 CO(1-0) Luminosity

Using the emission spectra in Fig. 1, we determine the CO(1-0) luminosities of the lines. Using the same method as Solomon et al. (1997), we derive the luminosity from the integrated flux of the emission line using Eqn. 1:

$$L'_{\text{CO}(1-0)} = 3.25 \times 10^7 \times S_{\text{CO}} \delta V \times \frac{D_L^2}{v_{\text{obs}}^2 (1+z)^3}, \quad (1)$$

where S_{CO} is the integrated flux density of the line (Jy), δV is the velocity width (km s^{-1}) and D_L is the luminosity distance to the galaxy (Mpc). $L'_{\text{CO}(1-0)}$ is in units of $\text{K km s}^{-1} \text{ pc}^2$, which can be converted to $L_{\text{CO}(1-0)}$ (in units of L_{\odot}) by $L/L' = (8\pi k_B/c^2) v_{\text{rest}}^3$, where k_B is the Boltzmann constant and c is the speed of light. Assuming that the CO gas and H_2 gas originate from the same reservoir (Ivion et al. 2010), such that the CO gas trace the H_2 gas, we can convert the luminosity of the CO(1-0) gas to the H_2 mass using:

$$M(\text{H}_2) = \alpha L'_{\text{CO}}, \quad (2)$$

where $M(\text{H}_2)$ is the mass of the H_2 region in M_{\odot} , L'_{CO}

⁵ Faint images of the radio sky at twenty-cm

Table 2. Bolometric luminosity (Tsai et al. 2015), CO(1–0) luminosity, FWHM of the Gaussian fit for CO(1–0) and estimated H₂ masses. The L_{bol} values are likely to be lower limits, and the uncertainties of 14% – 26% are in consideration of the difference between the power-law connection method (Tsai et al. 2015) and a more sophisticated continuous temperature model. See Section 3.1 for values marked with α for calculation.

ID	L _{bol} (10 ¹³ L _⊙)	L'_{CO(1–0)} (10 ¹⁰ K km s ^{–1} pc ²) α	FWHM _{CO(1–0)} (km s ^{–1})	M(H ₂) (10 ¹⁰ M _⊙) α
W0116–0505	11.7 ± 2.0	0.43 ± 0.15	75 ± 32	0.34 ± 0.12
W0410–0913	16.8 ± 2.4	2.60 ± 0.06	180 ± 77	2.08 ± 0.05
W0831+0140	18.0 ± 4.1	2.21 ± 0.15	342 ± 146	1.77 ± 0.12
W1322–0328	10.1 ± 1.4	0.37 ± 0.09	107 ± 47	0.30 ± 0.07
W2305–0039	13.9 ± 3.6	1.04 ± 0.11	137 ± 59	0.83 ± 0.09

Table 3. Continuum values for the five Hot DOGs observed with ALMA (S_{ALMA}) (see Fig. 3) and the continuum values for all five Hot DOGs for the VLA (S_{1cm}). ν_{VLA} shows the range of frequencies observed in the VLA observations. The final column gives the flux ratio of the line to continuum for each Hot DOG.

ID	S _{ALMA} (μ Jy)	S _{1cm} (μ Jy)	ν_{VLA} (GHz)	S _{CO(1–0)} /S _{1cm}
W0116–0505	241 ± 49	5.36 ± 2.07	27.6–28.6	29.0 ± 15.1
W0410–0913	716 ± 66	6.01 ± 1.21	24.5–25.5	131.9 ± 26.7
W0831+0140	435 ± 47	8.67 ± 1.76	23.0–24.0	66.7 ± 14.3
W1322–0328	140 ± 26	15.5 ± 0.84	27.9–28.9	3.8 ± 0.9
W2305–0039	283 ± 35	73.8 ± 3.55	27.5–28.5	7.0 ± 0.8

is the luminosity of the emission line in K km s^{–1} pc² and $\alpha \sim 0.8$ is the conversion factor, valid for ULIRGs and mergers (Downes & Solomon 1998; Bolatto et al. 2013). The results are shown in Table 2 for the five Hot DOGs in our sample. We see CO(1–0) luminosities $\gtrsim 0.4 \times 10^{10}$ K km s^{–1} pc², similar to findings by Ivison et al. (2010) and Riechers et al. (2011) for ULIRGs at similar redshifts. We compare the properties of the CO(1–0) luminosity with galaxies at similar redshifts in Fig. 4. We see that the Hot DOGs in our sample do not follow the expected trend with respect to the $\frac{L_{\text{CO(1–0)}}}{L_{\text{IR}}}$ ratio, suggesting that these galaxies are significantly more luminous in the IR than expected based on their L_{CO(1–0)}. This implies that the cold gas reservoirs in these Hot DOGs are different to other galaxy populations considered here. However, it should be noted that the L_{IR} is boosted above what would be expected for galaxies, supported by Fig. 4. We find a mean $\frac{L_{\text{CO(1–0)}}}{L_{\text{IR}}}$ value of $7.6 \pm 1.7 \times 10^{-10}$ which is significantly lower than the value of $4.2 \pm 0.5 \times 10^{-8}$ found by Thomson et al. (2012) for their two SMGs. The L_{IR} error for the 5 Hot DOGs in this sample is estimated by comparing the L_{IR} in Tsai et al. (2015) and a continuous temperature model, and the L_{bol} values shown in Table 2 are likely to be lower. This suggests that the Hot DOGs are significantly more luminous in the IR than would be expected for galaxies at this redshift for a given L_{CO(1–0)}.

We see agreement between the Hot DOGs and comparison samples with respect to the width of the CO(1–0) emission, suggesting that the width of the emission does not substantially deviate from expectations with respect to the luminosity of the line. As expected, the L'_{CO(1–0)} emission from these Hot DOGs is fainter than SMGs at $z=2.2$ – 2.5 in Ivison et al. (2011), suggesting that the cold molecular gas in the Hot DOGs is less luminous than SMGs at lower redshifts. In Fig. 1 we see that most of the Hot DOGs in our sample have CO(1–0) line widths $\lesssim 500$ km s^{–1}. The full width at zero intensity (FWZI) values reported in Thomson et al. (2012), ~ 500 – 1000 km s^{–1}, are significantly greater, showing that the Hot DOG CO(1–0) lines are narrower than

in typical SMGs. Comparing to VLA observations of lensed galaxies by Riechers et al. (2011), which report line widths of $\gtrsim 1300$ km s^{–1}, the Hot DOGs have similar line widths to optically selected QSOs. It should be noted that Farrah et al. (2017) show that Hot DOGs are unlikely to show any lensing, and it is therefore unlikely that the deviation in the L'_{CO}–L_{IR} relationship shown in Fig. 4 is due to lensing and is most likely attributed to the hot dust emission from an AGN present in this sample.

Follow-up observations by Wu et al. (2014) attempted to determine the cold molecular gas content of two Hot DOGs using the sub-millimetre array (SMA) and the combined array for research in millimetre-wave astronomy (CARMA), using CO(3–2) and CO(4–3) transitions. Wu et al. (2014) found masses of < 3.3 and $< 2.3 \times 10^{10}$ M_⊙ for W0149+2350 and W1814+3412 respectively. Comparing these results with the CO(1–0) masses in Table 2, we see general agreement for W0116–0505, although the other galaxies in our sample are significantly more massive, suggesting Hot DOGs do not have similar cold molecular gas contents. ALMA observations by Fan et al. (2018) for three Hot DOGs using CO(4–3) emission (including W0410–0913) suggest L'_{CO(4–3)} in the range of 10^{10} – 10^{11} L_⊙. Unfortunately, the CO(4–3) line for W0410–0913 in Fan et al. (2018) appears to be clipped, such that the full CO(4–3) emission line is outside the observed range, and so we are unable to comment on whether the use of a conversion factor would show agreement with this work. However, we see that the CO(4–3) line for W0410–0913 appears in the same velocity range as expected from these observations, but has a significantly broader FWHM in the CO(4–3) observations (330 – 560 km s^{–1}) compared to the CO(1–0) observations in this work (180 km s^{–1}).

3.2 Rest Frame 115.3 GHz Continuum

We measure the continuum flux for the five Hot DOGs in our sample using the *spws* away from the emission line, ~ 0.83 GHz in bandwidth and use the same single pixel posi-

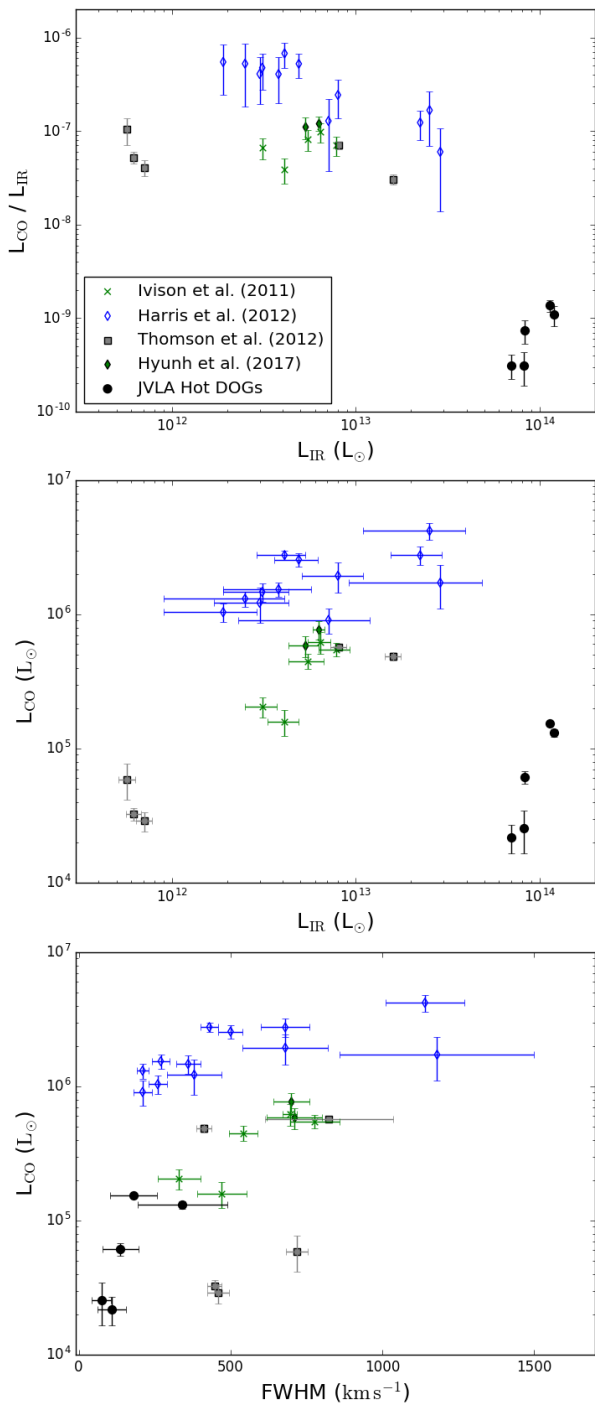


Figure 4. Comparison of the $L_{\text{CO}(1-0)}$ properties of the galaxies in our sample with other galaxies at high redshift. Top: The $L_{\text{CO}(1-0)}/L_{\text{IR}}$ ratio against L_{IR} . Middle: Comparison of the $L_{\text{CO}(1-0)}$ against L_{IR} . Bottom: $L_{\text{CO}(1-0)}$ against the FWHM of the CO(1–0) emission line. In each, we compare against $z = 2.2 - 2.5$ ALMA-selected SMGs (Ivison et al. 2011) (green crosses), lens-corrected DSFGs ($2.1 \leq z \leq 3.5$) (Harris et al. 2012) (blue empty diamonds), strongly lensed (corrected) SMGs at $z = 2.5 - 3$ (Thomson et al. 2012) (grey squares), and ALMA selected, Australian Telescope Compact Array observed galaxies at $z = 2.0232$ and 2.1230 respectively (Huynh et al. 2017) (green filled diamonds). VLA-observed Hot DOGs are illustrated by black filled circles.

tion used to extract the spectra for each target. The images of the continuum are shown in Fig. 5 and continuum fluxes are listed in Table 3. W2305-0039 has the brightest continuum emission, with the other four more weakly detected. The significantly greater continuum value for W2305-0039 could suggest additional dust or synchrotron/free-free emission processes, as discussed in Section 5.1.

K- and Ka-band radio observations for high-redshift galaxies are rare, and so a comparison with related observations is difficult. Our fluxes are 10 – 50% of those obtained by Aravena et al. (2016) for five lensed DSFGs selected using CO(1–0) emission within a redshift range of $z = 2 - 3$. We compute a mean continuum flux for the Hot DOGs of $23.6 \pm 11.5 \mu\text{Jy}$, indicated in Fig. 6, compared with $143 \pm 29 \mu\text{Jy}$ for the lensed DSFGs in Aravena et al. (2016). We see a similar result for when comparing two SMGs ($z = 2.5 - 3$) from Thomson et al. (2012) with values of $42 \pm 20 \mu\text{Jy}$ and $57 \pm 25 \mu\text{Jy}$. This suggests that the amount of cold molecular gas in these Hot DOGs is significantly lower than DSFGs and SMGs. This is surprising, given the very different nature of the cold gas in galaxies in our sample compared to typical SMGs and DSFGs at their respective redshifts.

4 SPECTRAL ENERGY DISTRIBUTIONS

Using archival data in addition to our VLA observations, we produce SEDs of the five Hot DOGs in our sample. We have included ALMA continuum data at $\lambda_{\text{obs}} \approx 700 \mu\text{m}$ ($\lambda_{\text{obs}} \approx 434 \mu\text{m}$ for W0410-0913), and *Herschel* PACS and SPIRE (observed frame $70 \mu\text{m}$, $160 \mu\text{m}$, $250 \mu\text{m}$, $350 \mu\text{m}$, $500 \mu\text{m}$) data from Tsai et al. (2015). We have also added data from *Warm-Spitzer* IRAC1 ($3.6 \mu\text{m}$) and IRAC2 ($4.5 \mu\text{m}$) (Griffith et al. 2012), *WISE* ($3.4 \mu\text{m}$, $4.6 \mu\text{m}$, $12 \mu\text{m}$ and $22 \mu\text{m}$), *Bolocam* (1 mm) (Wu et al. 2012) and 21 cm data from FIRST (White et al. 1997). For W0831+0140, we include continuum data from SCUBA-2 ($850 \mu\text{m}$; Jones et al. 2014) and ALMA CII ($\sim 387 \text{ GHz}$) observations (González-López et al. in prep). For W0410-0913, we include SHARC-II $350 \mu\text{m}$ observations (see Wu et al. 2012). The resulting SEDs are presented in Fig. 6.

We fit two separate models to the data, initially fitting a modified blackbody given by $S_\nu \propto \nu^{3+\beta} / (e^{h\nu/k_B T_{\text{dust}}} - 1)$ between $300 \text{ GHz} \lesssim \nu_{\text{obs}} \lesssim 2 \text{ THz}$. This frequency range is used in all of the SEDs except W0410-0913, in which we see a different distribution of dust temperatures than the rest of the targets. Thus, we chose to fit the modified blackbody between $300 \text{ GHz} \lesssim \nu_{\text{obs}} \lesssim 0.7 \text{ THz}$ for this target. After the fitting is performed, the dust emission is extrapolated to $\nu = 115 \text{ GHz}$ and subtracted from the VLA flux, and after this a single power-law is fitted ($\nu_{\text{obs}} < 300 \text{ GHz}$) to estimate the synchrotron emission from these galaxies. A standard Monte-Carlo Markov Chain (MCMC) Metropolis-Hastings routine (see e.g.; Robert 2015) is used to fit both models to the data, and the resulting curves from the blackbody and synchrotron power-law are combined with power-laws at $\nu_{\text{obs}} \gtrsim 2 \text{ THz}$ to produce the final spectral fit (Fig. 6). A single blackbody fit is necessary to accurately model the dust at increasing T_{dust} , and for consistency with previous work, we fix $\beta = 1.5$ (Blain et al. 2003; Wu et al. 2012) for all galaxies except W0410-0913, in which we find $\beta \sim 3$, due to the lower frequency peak in the SED. The resulting error

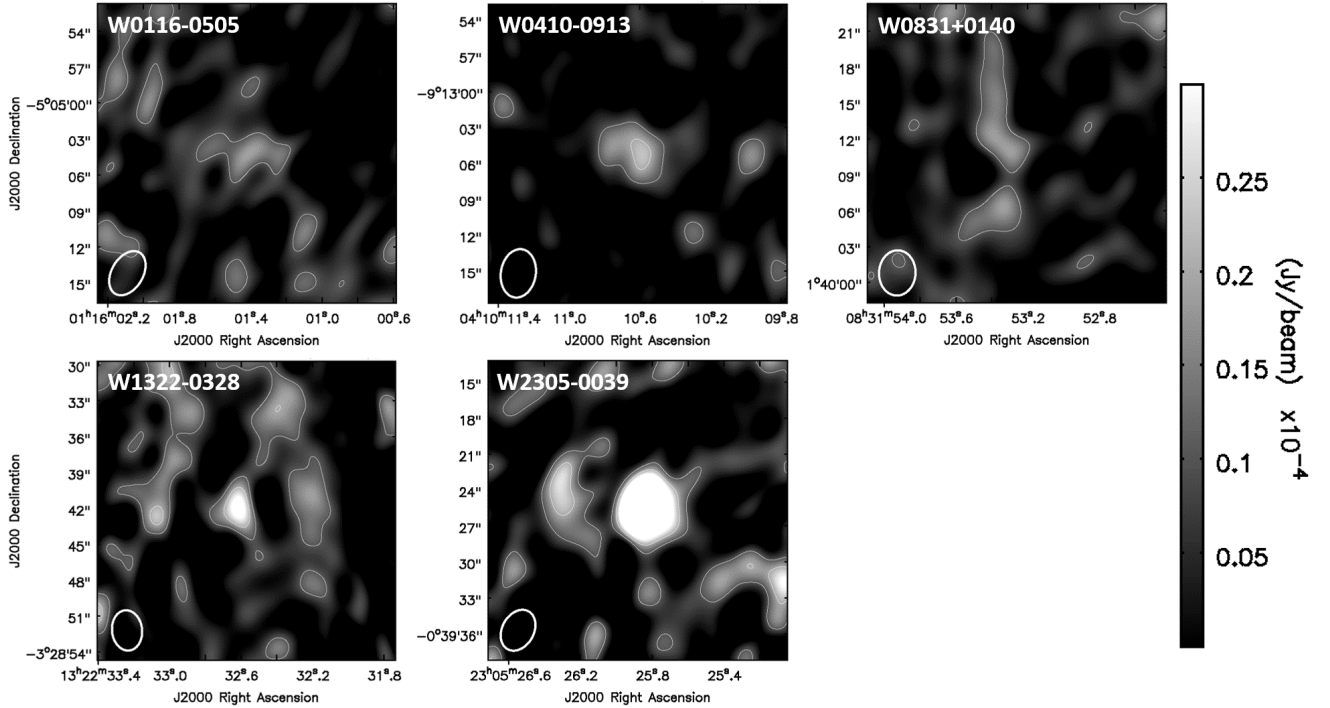


Figure 5. Continuum images (moment=0) for (left to right, top to bottom) W0116-0505, W0410-0913, W0831+0140, W1322-0328 and W2305-0039. Contours show the $0.1\ \mu\text{Jy}$, $0.2\ \mu\text{Jy}$ and $0.3\ \mu\text{Jy}$ levels, the peak continuum emission for these Hot DOGs. An ellipse in the bottom left-hand corner of each image illustrates the synthesized beam for each image.

in the normalisation and temperature parameters are shown in Fig. 7 and Table 4 for the blackbody fit.

As described above, we use a power-law to fit the FIRST and dust-subtracted VLA continua. Given the limited constraint provided by the data, we fix the slope to a value of $\alpha = -0.8$, typical for synchrotron emission (Condon 1992; Carilli & Yun 1999; Lacki et al. 2010), except for W2306-0039, for which we find a value of $\alpha = -1.23 \pm 0.02$. Upon determining the combined synchrotron and FIR-radio fits, we also attempt to determine the maximum level of free-free emission of these galaxies, assumed to follow the form $S_\nu \propto \nu^{-0.1}$, which could dominate between dust-dominated and synchrotron-dominated emission. The maximum permitted fluxes for the free-free emission, shown in Table 4, are affected by our assumption of the value of α and the error in the parameters for the FIR-radio blackbody model (see Fig. 7).

From the SEDs of the five Hot DOGs in our sample, we find that most 20 – 30 GHz VLA continuum fluxes are consistent with synchrotron and free-free emission ($S_\nu \propto \nu^{-0.1}$), with only a small potential contribution from dust in a few cases. Without additional radio fluxes, we are unable to determine which feature is dominant at rest-frame 115 GHz for these galaxies. W2305-0039 is the exception. W2305-0039 has a significant FIRST detection, likely caused by additional synchrotron emission, possibly dominating thermal dust in the VLA observations. As shown by the fit in Fig. 6, it is likely that the rest-frame 115.3 GHz free-free emission in W2305-0039 is dominated by synchrotron emission.

We list the 21 cm fluxes from the synchrotron fits at $\nu_{\text{obs}} \lesssim 300\ \text{GHz}$ with 1σ errors in Table 4, using a fixed spectral slope of $\alpha = -0.8$. The results suggest that the ex-

pected fluxes are close to the specific RMS of the FIRST images at the location of our targets, except for W0410-0913, which only appears in the area of the NRAO VLA Sky Survey (NVSS; Condon et al. 1998). These values are significantly lower than the reported depth of the FIRST catalogue ($\sim 1\ \text{mJy}$) by a factor of 8–30, and are likely to be more precise upper limits for all galaxies in our sample, except W0410-0913. Recent findings by Laor et al. (2019) suggest that galaxies with a higher Eddington ratio may have a steeper spectral index, and given that Tsai et al. (2015) found that these Hot DOGs should have an Eddington ratio ~ 1 , it is likely that the 21 cm flux estimate for W0410-0913, shown in Table 4, is an underestimate. This is further evidenced by the only target detected in FIRST, W2305-0039, which has a fitted spectral index of $\alpha = -1.23 \pm 0.02$. Deeper cm-wavelength observations could be used to understand the nature of the synchrotron emission in these galaxies and also further constrain maximum fluxes from free-free emission and 21 cm emission.

Using the fits for the full spectrum (e.g. Fig. 8), we estimate the bolometric and IR luminosities to compare with previous work (see Table 4). For the IR luminosity, measured between $8\ \mu\text{m}$ and 1 mm, we see no significant deviation in the luminosity estimate compared with Tsai et al. (2015) for all galaxies in our sample. The small increase is likely due to the data at lower-frequencies included in this work and the small deviation in the blackbody fits between these two works.

Comparing the dust temperatures between $160\ \mu\text{m}$ – 20 cm from our modified blackbody fits to Wu et al. (2012) for W0116-0505 and W0410-0913, we find lower values. Wu et al. (2012) used a similar blackbody fitting method for

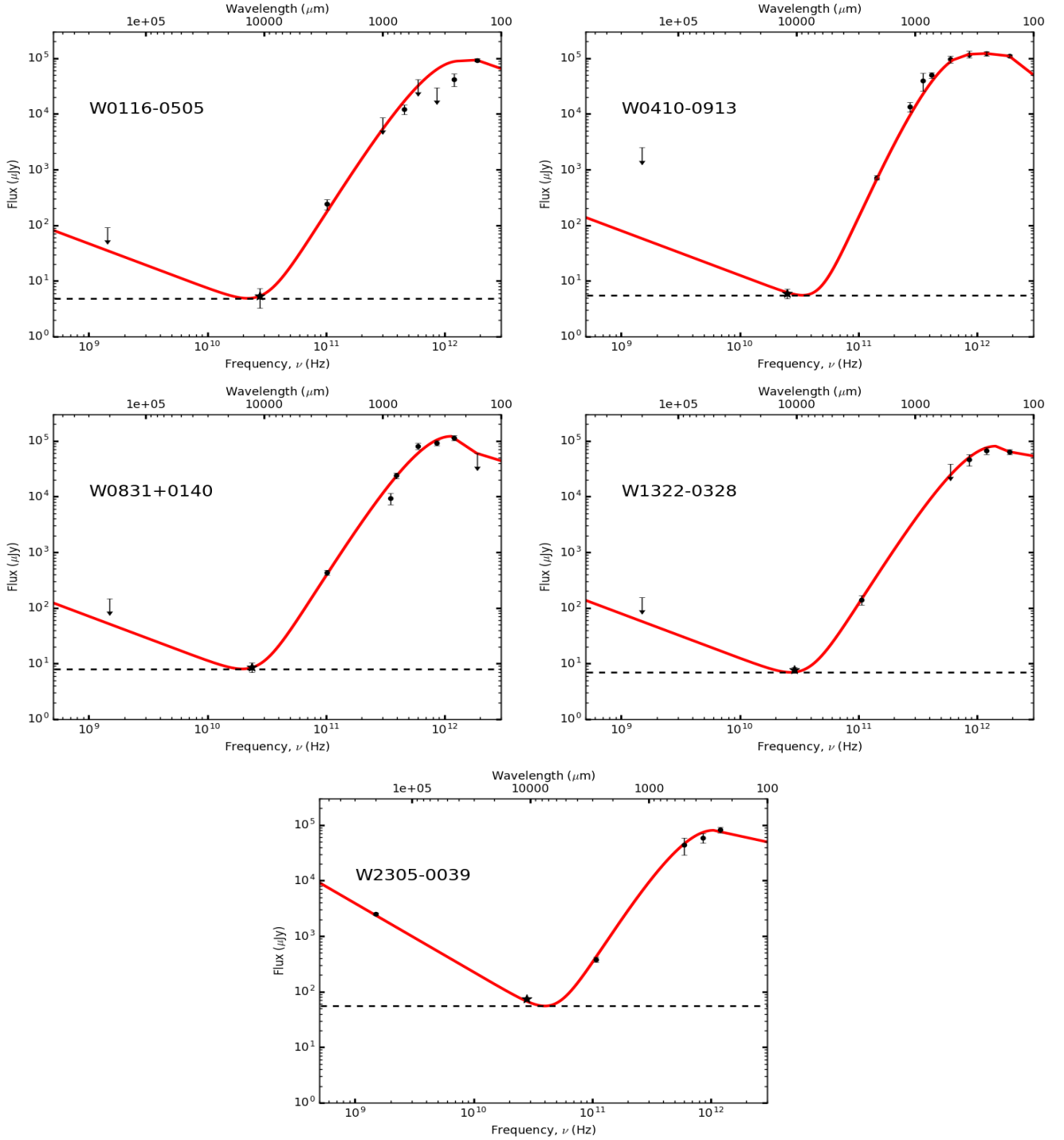


Figure 6. Observed frame SEDs of the five Hot DOGs in our sample. A single temperature blackbody was fitted to the $160\mu\text{m}$ to 2cm data, and further power-laws were added to fit the remaining data. Radio data, constrained by VLA and FIRST data, is fitted by a single power-law ($S_\nu \propto \nu^{-0.8}$), except for W2305-0039, and the resultant curve is shown by a solid red line. A star has been used to denote the VLA data in each SED and a dashed line indicates the maximum level of free-free emission (see Table 4).

$8\mu\text{m}$ to $1000\mu\text{m}$ data, and found dust temperatures of $123 \pm 8\text{K}$ and $82 \pm 5\text{K}$ for W0116-0505 and W0410-0913 respectively. These are 1–3 times the values shown in Table 4. While our results differ significantly from Wu et al. (2012), we fit the coldest dust using previously unavailable data from ALMA and the VLA. Furthermore, our results

focus on the temperature of the coldest dust on the Rayleigh-Jeans tail, and it is unlikely that our results significantly underestimate the temperature of the coldest dust in these galaxies.

Fig. 6 shows that W2305-0039 is the only galaxy of our sample with significant 1.4 GHz radio emission. We fit a spec-

Table 4. The fitted temperatures for the FIR-radio blackbody curve between $160\mu\text{m}$ and 2cm in Fig. 6 and the inferred 21cm and $850\mu\text{m}$ fluxes. All values in this table are inferred from the fits in Fig. 6. We show the maximum possible flux contribution from free-free emission (S_{ff}). The final two columns show the q_{IR} values, discussed in Section 5.2 (Eqn. 3) and the reduced χ^2 values for the SED fits. Data marked with ($^{\alpha}$) have fitted points which can be compared with observations.

ID	T (K)	$S_{21\text{cm}}$ (μJy)	$S_{850\mu\text{m}}$ (mJy)	S_{ff} (μJy)	L_{bol} ($10^{13}L_{\odot}$)	L_{IR} ($10^{13}L_{\odot}$)	q_{IR}	χ^2
W0116-0505	69^{+4}_{-5}	36.5 ± 9.2	8.4 ± 3.6	< 4.87	13.4	9.13	> 2.63	1.49
W0410-0913	32 ± 3	62.3 ± 6.7	23 ± 3	< 5.53	17.7	11.2	2.75 ± 0.11	0.75
W0831+0140	60^{+6}_{-5}	55.3 ± 10.3	$17\pm 2.7^{\alpha}$	< 8.01	18.9	11.2	> 2.35	0.69
W1322-0328	62^{+6}_{-4}	61.7 ± 5.5	6.1 ± 2.3	< 6.96	10.7	7.06	> 2.30	0.13
W2305-0039	47 ± 3	$2668.6\pm 519.6^{\alpha}$	14 ± 1.6	< 55.28	14.4	7.57	0.85 ± 0.22	0.37

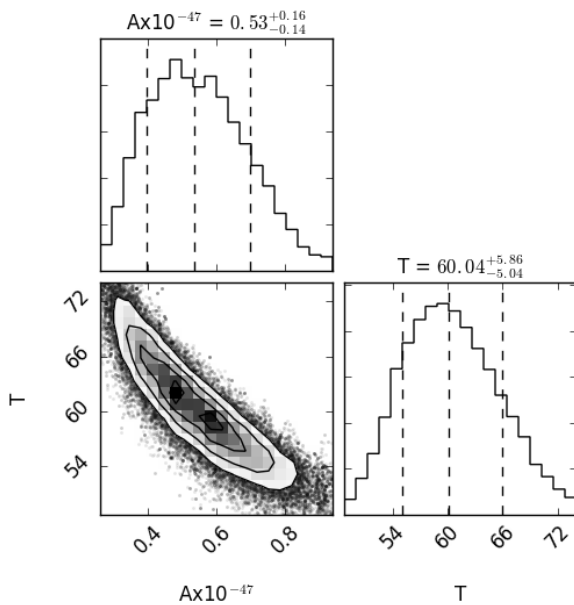


Figure 7. The fitted FIR-radio SED parameters for a member of our sample (W0831+0140) using the single-temperature blackbody model. Dashed lines show the -1σ , median and 1σ . The A parameter is the normalisation and T is the temperature (K).

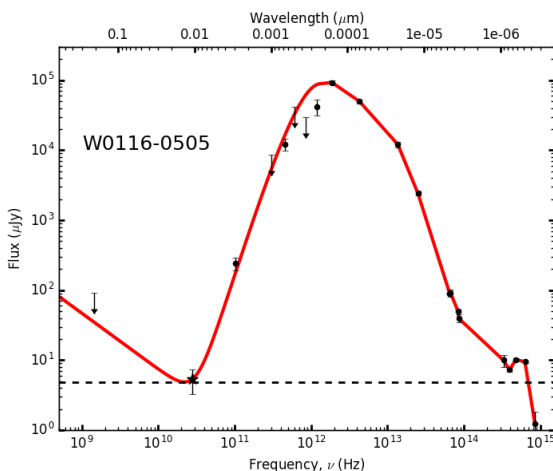


Figure 8. The full SED for an example galaxy (W0116-0505). The values from the fits were used to determine the K-corrected FIR luminosity, shown in Section 5.2.

tral index of $\alpha = -1.23 \pm 0.02$ by combining FIRST fluxes with our VLA observations, significantly steeper than most values of α (Condon 1992). This spectral index is significantly greater than that determined via a stacking analysis of $z \sim 2$ galaxies in Magnelli et al. (2015), and using the definition for radio-loudness in Stern et al. (2000), W2305-0039 is radio-loud compared to the other Hot DOGs in our sample. This is not surprising, given that 10 – 15% of galaxies are expected to be radio-loud (Kratzer & Richards 2015), and could suggest that there is a subset of radio-loud Hot DOGs.

The maximum value of the free-free emission is $\lesssim 3\mu\text{Jy}$ for the Hot DOGs in our sample, and significantly greater for W2305-0039 due to the lower value of α used, though its value is likely to be much lower given the dominance of its synchrotron emission. The maximum values are lower than the values calculated in Thomson et al. (2012), which found, for two SMGs, values of $12\mu\text{Jy}$ and $24\mu\text{Jy}$. This implies that the Hot DOGs have lower free-free emission than typical SMGs and suggests that these galaxies could have lower star-formation rates than SMGs at lower redshifts. However, the limited number of sources precludes a statistical assessment of whether this is characteristic of the entire Hot DOG population, and if so, whether this is due to the greater activity of the AGN or the surrounding environment.

5 DISCUSSION

5.1 30 GHz Emission from Hot DOGs

Our VLA data for five Hot DOGs are near the expected continuum flux from a dust-emission power-law ($S \propto \nu^{2+\beta}$), and we find that dust emission could provide a mean $\sim 20\%$ of the VLA flux. At 1.4 GHz, we predict a distinct lack of emission in 4/5 galaxies in our sample, as shown in Fig. 6. To understand whether there is any emission just beneath the noise level of FIRST, we stack the FIRST images for W0116-0505, W0126-0529, W0831+0140 and W1322-0328. The Root-Mean-Square (RMS) values for the individual images are a third of the 1.4 GHz flux for W2305-0039, however we see no stacked detection (Fig. 9), suggesting that the 1.4 GHz emission of these galaxies is substantially lower than the detection limit of FIRST. It is unlikely that the dust emission from these Hot DOGs is suppressing the synchrotron processes at 1.4 GHz, and it is more likely that these Hot DOGs are relatively radio-quiet compared to W2305-0039.

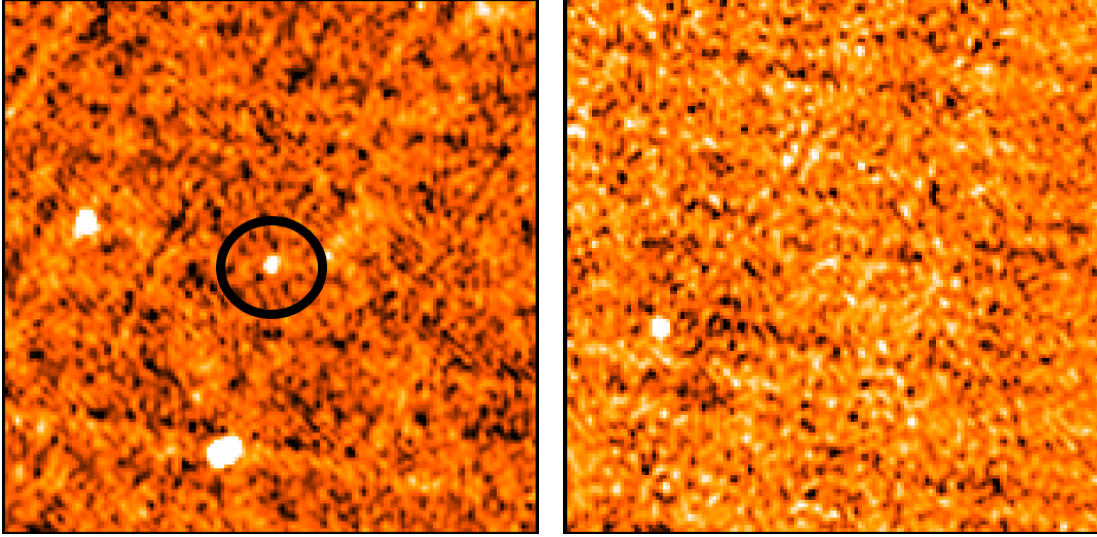


Figure 9. Left: Image of the W2305-0039 field using FIRST image cutout service. The Hot DOG in the field has been ringed. Right: Stacked FIRST images of W0116-0505, W0126-0529, W0831+0140 and W1322-0328, showing that no net flux is visible at 1.4GHz. W0410-0913 has not been included in this process as it is outside the FIRST survey coverage. Both images constitute $4.5' \times 4.5'$ fields.

5.2 FIR-Radio Correlation

The FIR-radio correlation has been widely used to identify star formation properties of galaxies at high redshift (see Lacki & Thompson 2010, for a review). Star formation drives the correlation, in which dust-obscured stellar emission produces flux in the FIR, while SNe from the same stars with masses $M_{\odot} \gtrsim 8M_{\odot}$ produce synchrotron emission at ~ 1.4 GHz. The q_{IR} value is used to compare the difference in the emission, given by:

$$q_{\text{IR}} = \log_{10} \left(\frac{L_{\text{FIR}}}{3.75 \times 10^{12} \times S_{1.4\text{GHz}}} \right), \quad (3)$$

where L_{FIR} is the rest-frame FIR luminosity in W m^{-2} , and $S_{1.4\text{GHz}}$ is the flux at rest-frame 1.4 GHz in $\text{W m}^{-2} \text{Hz}^{-1}$. The correlation is well documented locally (van der Kruit 1971; Helou et al. 1985; Condon 1992; Yun et al. 2001), and extending to higher redshifts (Lacki et al. 2010; Ivison et al. 2010), with Thomson et al. (2014) finding $q_{\text{IR}} = 2.56 \pm 0.05$ using ALMA $870 \mu\text{m}$ observations for ~ 50 $z \gtrsim 2$ SMGs. Ivison et al. (2010) found a similar $q_{\text{IR}} = 2.40 \pm 0.24$ for *Herschel* $250 \mu\text{m}$ -selected galaxies at $z > 1$, and Boyle et al. (2007) discovered that the correlation was constant down to μJy fluxes for radio-quiet quasars.

To estimate the value of the q_{IR} for the FIRST undetected Hot DOGs in our sample, we assume $S \propto \nu^{\alpha}$ where $\alpha = -0.8$ for synchrotron emission to extrapolate the expected value at 1.4 GHz from the VLA detections. This extrapolation is necessary due to their non-detections (for 4/5 galaxies) in FIRST. As previously discussed, Laor et al. (2019) suggest that galaxies with a higher Eddington luminosity may have steeper spectral indices, and could suggest that we have underestimated the 1.4 GHz fluxes of our sample. However, without additional observations, we cannot determine the true value of the rest-frame 1.4 GHz emission. We see no significant deviation in the q_{IR} values for these galaxies using the L_{FIR} values from Tsai et al. (2015), which

is expected given that our L_{FIR} values deviate by only $\sim 15\%$ at most.

We compute the q_{IR} values for the Hot DOGs in our sample using the SED fits of the FIR within the wavelength range $8\text{--}1000 \mu\text{m}$ (Ivison et al. 2010), as shown in Table 4. All of the galaxies undetected in FIRST/NVSS possess q_{IR} estimates within the upper 2σ limits from Ivison et al. (2010), $q_{\text{IR}} = 2.40 \pm 0.24$, suggesting that these galaxies may be radio-quiet. W0410-0913, undetected in NVSS, has a q_{IR} value estimated using the assumption that the radio spectral index is $\alpha = -0.8$. However, it should be noted that, given the more relaxed constraints in NVSS, the q_{IR} value could be significantly affected by this assumption, and may possess a q_{IR} value similar to W2305-0039. Using our assumption, we see that W0410-0913 has a q_{IR} value above the 2σ limits from Ivison et al. (2010), suggesting that this Hot DOG is radio-quiet with respect to the FIR emission. The lack of radio-emission from these undetected galaxies is unusual, given that the obscured emission in the FIR from the presence of an AGN should be expected to also radiatively boost the radio emission. The higher q_{IR} values from W0116-0505 and W0410-0913 are likely due to dust significantly boosting the FIR emission, while the radio emission is unaffected. The q_{IR} value for W2305-0039 ($q_{\text{IR}} = 0.85 \pm 0.22$) is at least an order of magnitude smaller than the mean $z = 2$ value from Ivison et al. (2010), suggesting that W2305-0039 is more radio-loud than expected for SMGs, and thus that the galaxies in our sample are all different from the population observed in previous work on the high-redshift FIR-radio correlation.

Schleicher & Beck (2013) and Schober et al. (2016) suggest a break down of the FIR-radio correlation at high redshifts due to more effective electron cooling by Bremsstrahlung emission in the cosmic microwave background. This is unlikely to be the cause of the increased q_{IR} values in the NVSS/FIRST undetected galaxies in our sample, given that the radiation field of the galaxies will dominate over the cosmic microwave background, and this

effect should only dominate at $z \gtrsim 5$. The higher q_{IR} values for the Hot DOGs in our sample are likely due to the increased FIR emission from the dust-obscured AGN shown in previous work (Assef et al. 2015; Díaz-Santos et al. 2016), such that the AGN boosts the FIR-emission from young stars compared to normal galaxies.

If the central AGN is radio-quiet, the observed q_{IR} values from these galaxies would be dramatically increased. This is unexpected and it is likely that the dust has boosted the FIR emission above what would be expected, while the 1.4 GHz emission is similar to that of a normal galaxy at this redshift. A lack of synchrotron emission could also suggest an abundance of young stars that have not undergone a SNe event within these galaxies, and could suggest that these galaxies are still forming stars, which could explain the lower rest-frame 115.3 GHz continuum fluxes observed in Table 3. Magnelli et al. (2015) and Delhaize et al. (2017) suggest a weak redshift dependence in the FIR-radio correlation of the form $q_{\text{IR}}(z) = q_{\text{IR}}(1+z)^{-\beta}$, where $\beta \sim 0.15$. Using the values from Ivison et al. (2010), we expect to see $q_{\text{IR}}(z) \sim 2 \pm 0.15$ for the Hot DOGs in our sample, implying significantly greater radio fluxes than the FIRST limits suggest. These results were derived for star-forming galaxies, and so the FIR may be significantly enhanced by AGN emission in our sample, increasing the expected FIR emission beyond the radio emission produced from SNe. This agrees with previous results from SED fits of Hot DOGs (Jones et al. 2014; Assef et al. 2015), and further suggests that the AGN in these galaxies are radio-quiet.

To understand whether the q_{IR} values for our sample are typical for Hot DOGs or other classes of object, we compare our values with both high and low redshift galaxies, comparing q_{IR} values determined using the FIR luminosity between 8 – 1000 μm . We compare with 10 Hot DOGs from Jones et al. (2014), which used 850 μm SCUBA-2 data to search for companion SMGs around Hot DOGs. W0831+0140 is common to both works, and we expect that the Hot DOGs in Jones et al. (2014) have similar radio properties to the Hot DOGs in this work. To understand whether our q -values are typical of other dusty galaxies at this redshift, we compare with star-forming DSFGs from Shu et al. (2016) selected from the GOODS-N field, which have redshifts $z = 2-4$. We also compare with 52 ALMA 870 μm selected SMGs in the Extended Chandra Deep Field South with a redshift range of $z_{\text{phot}} \sim 0.4-4.7$ (median $z = 2.125$) from Thomson et al. (2014), which were observed using the VLA at 1.4 GHz at $> 3\sigma$ significance. The results are shown in Fig. 10, which illustrates the distribution of the q_{IR} values as a function of redshift.

Hot DOGs undetected in the FIRST survey from Jones et al. (2014) have q_{IR} values consistent with the Hot DOGs undetected in the FIRST survey from this work, suggesting that the non-detection of 1.4 GHz radio emission is typical for this class of dust-obscured galaxies. We find two Hot DOGs with detections in Jones et al. (2014), which have similar q_{IR} values to W2305-0039, suggesting a possible subclass of radio-loud Hot DOGs. It should be noted that these Hot DOGs have different selection criteria than the radio-WISE selected galaxies in Lonsdale et al. (2015), as shown by the selection comparison in Penney et al. (2019). There are Hot DOGs in both works without detections in FIRST, with lower limits for the q -values that agree with the median

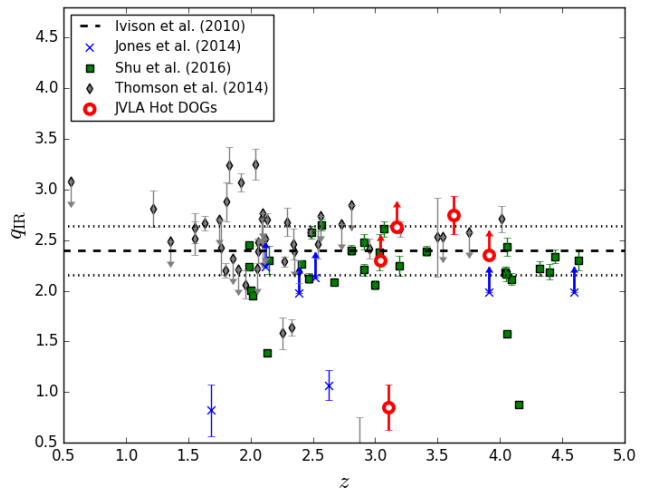


Figure 10. Comparison of q_{IR} values derived using rest-frame $L_{8-1000\mu\text{m}}$ and $S_{1.4\text{GHz}}$ for the Hot DOGs in our sample (red open circles) against previously observed Hot DOGs (Jones et al. 2014) (blue crosses). $L_{8-1000\mu\text{m}}$ was derived using the fits from the SEDs in Fig. 6. $S_{1.4\text{GHz}}$ values were K-corrected, using a spectral index of $\alpha = -0.8$. Comparison samples are shown by green squares and grey diamonds for star-forming DSFGs (Shu et al. 2016) and 870 μm selected SMGs (Thomson et al. 2014) respectively. A black dashed line and black dotted lines illustrate the median value and the $\pm 1.5\sigma$ values for 250 μm selected galaxies in the GOODS-N field (Ivison et al. 2010).

values for Ivison et al. (2010) and Thomson et al. (2014), suggesting that these galaxies could agree with the FIR-radio correlation. However, two Hot DOGs from this work (W0116-0505 and W0410-0913) have lower limits for their q_{IR} values close to the upper limit in Thomson et al. (2014), suggesting that the lower limits for the Hot DOGs could severely underestimate their true q_{IR} value. We see agreement between the three comparison works, showing that the distribution of q_{IR} values is observed in other galaxies with a wide range of selections and redshifts, but is generally not observed in Hot DOGs from this work and Jones et al. (2014), and that Hot DOGs have a wider spread of q_{IR} values than typical galaxies. It should be noted that the Hot DOGs in this work, except W0831+0140, differ from the Hot DOGs in Jones et al. (2014) due to the luminosity constraints in Tsai et al. (2015), but are expected to be the same class of galaxy. These results suggest that Hot DOGs are radio-quiet and the increased FIR luminosity has likely boosted the expected q_{IR} values within the upper 2σ values.

6 CONCLUSIONS

The results from the VLA observations of five WISE-selected, dusty, luminous obscured galaxies are:

- We formulate SEDs of the five Hot DOGs in our sample from archival data in conjunction with ALMA and VLA observations and a single modified blackbody and power-law models. We find that synchrotron/free-free emission dominates at the rest-frame 115.3 GHz for four of the galaxies in our sample, which show little or no dust contribution, and W2305-0039 contains additional synchrotron emission, in-

creasing the rest-frame 115.3 GHz fluxes above a single temperature blackbody model.

- We determine the CO(1–0) luminosity for the five Hot DOGs in our sample and compare with $z \sim 2$ SMGs from Ivison et al. (2011). We find that the Hot DOGs have significantly lower values for the CO(1–0) line luminosity, and may not possess significant cold molecular gas reservoirs compared with lower redshift, star-forming galaxies.

- We estimate the maximum free-free emission in the galaxies in our sample and compare to two $z \sim 2$ SMGs from Thomson et al. (2012). We find that the Hot DOGs have typically lower fluxes for free-free emission and may not possess as significant star formation activity as SMGs at lower redshifts.

- We determine that the q_{IR} values for the five Hot DOGs in our sample using SED fits, and find the galaxies undetected in FIRST have higher values compared with other galaxies at these redshifts. This suggests that the FIR has been boosted by the dust emission, significantly increasing q_{IR} . Thus, Hot DOGs are generally radio-quiet, and are dominated by strong FIR emission.

- We determine that W2305-0039 has an additional 115.3 GHz CO(1–0) radio companion. W2305-0039 likely has compact radio emission, rather than jets extending from the host galaxy, and is more radio-loud than the other Hot DOGs in our sample.

- We find redshifts in agreement with previous work by Tsai et al. (2015) for 4 Hot DOGs. For W0410-0913, we find a redshift outside the predicted error margins from previous work, but in agreement with new findings using ALMA. We find no CO(1–0) emission line in the spectra of W0126-0529 at the frequency corresponding to a previously known redshift, which was later updated to $z = 0.8301$ (Jun et al. 2020).

ACKNOWLEDGEMENTS

The authors wish to thank the staff in the Department of Physics and Astronomy at the Leicester University for their support. Jordan Penney is supported by the Science and Technologies Facilities Council (STFC) studentship. M. Kim was supported by the National Research Foundation of Korea (NRF), grant funded by the Korean government (MSIP) (No. 2017R1C1B2002879). R. J. Assef was supported by the FONDECYT grant (NO. 1191124). T.D.S. acknowledges support from the CASSACA and CONICYT fund CAS-CONICYT Call 2018. This research was carried out in part at the Jet Propulsion Laboratory, California Institute of Technology, under a contract with NASA. H.D.J. was supported by the Basic Science Research Program through the National Research Foundation of Korea (NRF) funded by the Ministry of Education (NRF-2017R1A6A3A04005158). C.-W. Tsai was supported by a grant from the NSFC (No. 11973051). The National Radio Astronomy Observatory is a facility of the National Science Foundation operated under cooperative agreement by Associated Universities, Inc. This publication makes use of data products from the *Wide-field Infrared Survey Explorer*, which is a joint project of the University of California, Los Angeles, and the Jet Propulsion Laboratory/California Institute of Technology, funded by the National Aeronautics

and Space Administration. This paper makes use of ALMA data ADS/JAO.ALMA#2017.1.00358.S. ALMA is a partnership of ESO (representing its member states), NSF (USA) and NINS (Japan), together with NRC (Canada), NSC and ASIAA (Taiwan), and KASI (Republic of Korea), in cooperation with the Republic of Chile. The Joint ALMA Observatory is operated by ESO, AUI/NRAO and NAOJ.

References

- Aravena M., et al., 2016, *MNRAS*, **457**, 4406
 Assef R. J., et al., 2015, *ApJ*, **804**, 27
 Barnes J. E., Hernquist L., 1992, *ARA&A*, **30**, 705
 Barnes J. E., Hernquist L., 1998, *ApJ*, **495**, 187
 Blain A. W., Smail I., Ivison R. J., Kneib J.-P., Frayer D. T., 2002, *Phys. Rep.*, **369**, 111
 Blain A. W., Barnard V. E., Chapman S. C., 2003, *MNRAS*, **338**, 733
 Bolatto A. D., Wolfire M., Leroy A. K., 2013, *ARA&A*, **51**, 207
 Boyle B. J., Cornwell T. J., Middelberg E., Norris R. P., Appleton P. N., Smail I., 2007, *MNRAS*, **376**, 1182
 Carilli C. L., Yun M. S., 1999, *ApJ*, **513**, L13
 Condon J. J., 1992, *ARA&A*, **30**, 575
 Condon J. J., Cotton W. D., Greisen E. W., Yin Q. F., Perley R. A., Taylor G. B., Broderick J. J., 1998, *AJ*, **115**, 1693
 Conselice C. J., 2014, *ARA&A*, **52**, 291
 Cutri R. M., et al., 2012, Explanatory Supplement to the WISE All-Sky Data Release Products, Explanatory Supplement to the WISE All-Sky Data Release Products
 Delhaize J., et al., 2017, *A&A*, **602**, A4
 Díaz-Santos T., et al., 2016, *ApJ*, **816**, L6
 Díaz-Santos T., et al., 2018, *Science*, **362**, 1034
 Downes D., Solomon P. M., 1998, *ApJ*, **507**, 615
 Eisenhardt P. R. M., et al., 2012, *ApJ*, **755**, 173
 Fan L., Knudsen K. K., Fogasy J., Drouart G., 2018, *ApJ*, **856**, L5
 Farrah D., et al., 2017, *ApJ*, **844**, 106
 Faucher-Giguère C.-A., Quataert E., 2012, *MNRAS*, **425**, 605
 Griffith R. L., et al., 2012, *AJ*, **144**, 148
 Harris A. I., et al., 2012, *ApJ*, **752**, 152
 Helou G., Soifer B. T., Rowan-Robinson M., 1985, *ApJ*, **298**, L7
 Hopkins P. F., Hernquist L., Cox T. J., Kereš D., 2008, *ApJS*, **175**, 356
 Huynh M. T., et al., 2017, *MNRAS*, **467**, 1222
 Ivison R. J., et al., 2010, *A&A*, **518**, L31
 Ivison R. J., Papadopoulos P. P., Smail I., Greve T. R., Thomson A. P., Xilouris E. M., Chapman S. C., 2011, *MNRAS*, **412**, 1913
 Jones S. F., et al., 2014, *MNRAS*, **443**, 146
 Jun H. D., et al., 2020, *The Astrophysical Journal*, **888**, 110
 Kormendy J., Bender R., 2012, *ApJS*, **198**, 2
 Kratzer R. M., Richards G. T., 2015, *AJ*, **149**, 61
 Lacki B. C., Thompson T. A., 2010, *ApJ*, **717**, 196
 Lacki B. C., Thompson T. A., Quataert E., 2010, *ApJ*, **717**, 1
 Laor A., Baldi R. D., Behar E., 2019, *MNRAS*, **482**, 5513
 Lonsdale C. J., et al., 2015, *ApJ*, **813**, 45
 Magnelli B., et al., 2015, *A&A*, **573**, A45
 McMullin J. P., Waters B., Schiebel D., Young W., Golap K., 2007a, in Shaw R. A., Hill F., Bell D. J., eds, *Astronomical Society of the Pacific Conference Series Vol. 376, Astronomical Data Analysis Software and Systems XVI*. p. 127
 McMullin J. P., Waters B., Schiebel D., Young W., Golap K., 2007b, *CASA Architecture and Applications*. p. 127
 Morton D. C., Noreau L., 1994, *ApJS*, **95**, 301
 Omont A., 2007, *Reports on Progress in Physics*, **70**, 1099

- Peñaloza C. H., Clark P. C., Glover S. C. O., Shetty R., Klessen R. S., 2017, *MNRAS*, **465**, 2277
- Penney J. I., et al., 2019, *MNRAS*, **483**, 514
- Perley R. A., Chandler C. J., Butler B. J., Wrobel J. M., 2011, *ApJ*, **739**, L1
- Riechers D. A., Hodge J., Walter F., Carilli C. L., Bertoldi F., 2011, *ApJ*, **739**, L31
- Robert C. P., 2015, arXiv e-prints, p. arXiv:1504.01896
- Sanders D. B., Mirabel I. F., 1996, *ARA&A*, **34**, 749
- Sanders D. B., Soifer B. T., Elias J. H., Madore B. F., Matthews K., Neugebauer G., Scoville N. Z., 1988, *ApJ*, **325**, 74
- Schleicher D. R. G., Beck R., 2013, *A&A*, **556**, A142
- Schober J., Schleicher D. R. G., Klessen R. S., 2016, *ApJ*, **827**, 109
- Schweizer F., Seitzer P., 1998, *AJ*, **116**, 2206
- Sheth K., Vogel S. N., Wilson C. D., Dame T. M., 2008, *ApJ*, **675**, 330
- Shu X. W., et al., 2016, *ApJS*, **222**, 4
- Solomon P. M., Downes D., Radford S. J. E., Barrett J. W., 1997, *ApJ*, **478**, 144
- Stern D., Djorgovski S. G., Perley R. A., de Carvalho R. R., Wall J. V., 2000, *AJ*, **119**, 1526
- Tacconi L. J., et al., 2008, *ApJ*, **680**, 246
- Thomson A. P., et al., 2012, *MNRAS*, **425**, 2203
- Thomson A. P., et al., 2014, *MNRAS*, **442**, 577
- Toomre A., 1977, *ARA&A*, **15**, 437
- Tsai C.-W., et al., 2015, *ApJ*, **805**, 90
- Werner M. W., et al., 2004, *ApJS*, **154**, 1
- White R. L., Becker R. H., Helfand D. J., Gregg M. D., 1997, *ApJ*, **475**, 479
- Wright E. L., et al., 2010, *AJ*, **140**, 1868
- Wu J., et al., 2012, *ApJ*, **756**, 96
- Wu J., et al., 2014, *ApJ*, **793**, 8
- Wylezalek D., et al., 2013, *ApJ*, **769**, 79
- Yun M. S., Reddy N. A., Condon J. J., 2001, *ApJ*, **554**, 803
- van der Kruit P. C., 1971, *A&A*, **15**, 110

APPENDIX A: APPENDIX

Here, we discuss the results for observations of W0126-0529, previously expected to be a Hot DOG at $z = 2.937$, later determined to be at $z = 0.8301$ (Jun et al. 2020) after the initial VLA observations were made. Given this lower redshift, W0126-0529 is not part of the subset of Hot DOG discussed in Eisenhardt et al. (2012) and has therefore been omitted from the main results of this paper. In Table A1, we provide measurements for W0126-0529 given the new redshift information.

We use the same calibration pipeline noted in Section 2, and use the same TCLEAN parameters in CASA to produce the spectral and continuum images, shown in Fig. A1. We use the *spw* corresponding to the redshift from Tsai et al. (2015). As expected, we find no CO(1–0) emission line at this frequency ($\nu_{\text{obs}} \sim 29.29$ GHz) as shown in Fig. A1, and there are no other lines within the observed frequency range for $z = 0.8301$, such that we cannot confirm the redshift identification of Jun et al. (2020). In Fig. A1 we observe a potential companion source, similar to W2305-0039, $\sim 5''$, below the expected position, however we find no emission spectra at this position consistent with the redshift in Tsai et al. (2015) and this is likely to be noise. The continuum image for W0126-0529 shows a single, bright object in the centre of the field, as expected, with a flux measurement

of $128 \pm 14.6 \mu\text{Jy}$, brighter than any of the continuum emission for the five Hot DOGs in this paper. The significantly brighter continuum emission for this object is likely due to the lower redshift, placing the VLA observations further along the Raleigh-Jean’s tail, closer to the peak in the FIR emission. We model the expected spectrum for this galaxy below.

Using the same method outlined in Section 4, we use archive data for W0126-0529 to construct an SED, shown in Fig. A2 to estimate the properties of the object, listed in Table A1. Unlike the Hot DOGs in Section 4, we used a lower β value of $\beta = 0.5$, which appeared to better fit the slope than the previously used value of $\beta = 1.5$ for the Hot DOGs. Understandably, this suggests that there is significantly less dust obscuration for this object than for the Hot DOGs in our sample, and could suggest that it is a normal-type galaxy. From the SED, we find a maximum free-free emission flux of $31.3 \mu\text{Jy}$, significantly greater than all of the Hot DOGs in our sample, except for W2305-0039, suggesting that W0126-0529 could possess large quantities of cold molecular gas. Additional observations at lower frequencies than these VLA observations are required to confirm this.

From the SED model of this galaxy, we are able to estimate the q_{IR} value, and find a value of $q_{\text{IR}} = 2.97 \pm 0.77$, suggesting that this galaxy is more radio-quiet than expected from previous work by Ivison et al. (2010). This is unusual, given the large quantities of cold molecular gas residing within this object, and could suggest that this object does not have significant AGN activity, as suggested in Jun et al. (2020).

This paper has been typeset from a $\text{\TeX}/\text{\LaTeX}$ file prepared by the author.

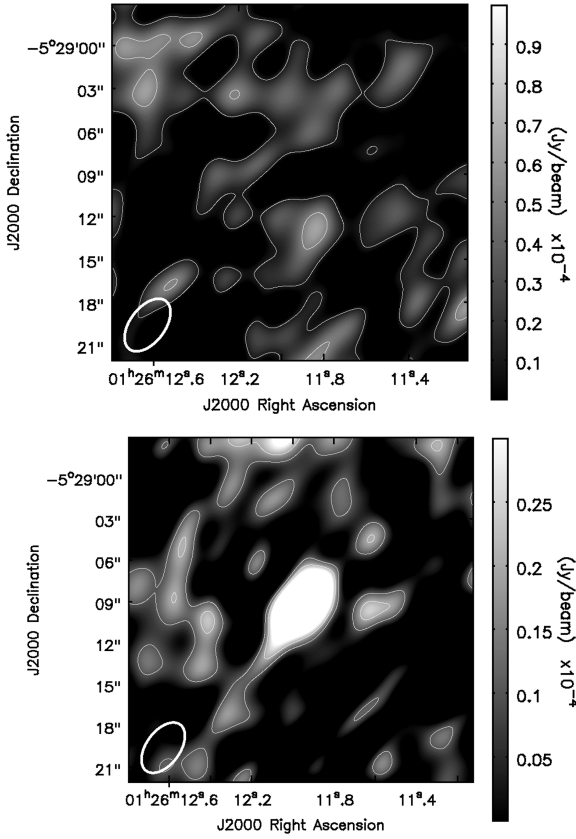


Figure A1. Emission line (top) and continuum image (bottom) for W0126-0529. Contours show the $0.1\mu\text{Jy}$, $0.5\mu\text{Jy}$, $1\mu\text{Jy}$ levels for the emission line image and the $0.1\mu\text{Jy}$, $0.2\mu\text{Jy}$ and $0.3\mu\text{Jy}$ levels for the continuum image. An ellipse in the bottom left-hand corner of both images illustrates the synthesized beam for the image.

Table A1. Observed and computed properties for W0126-0529, previously believed to be a HyLIRG Hot DOG during the time of the VLA observations (see Section 2). $S_{1\text{cm}}$ denotes the continuum flux for the galaxy using the same flux measurement method in Section 2, using all available *spws*. Computed properties using the SED in Fig. A2 below are also included.

W0126-0529	
RA (J2000)	01:26:11.95
DEC (J2000)	-05:29:09.1
z	0.8301
Major (arcsec)	4.17
Minor (arcsec)	2.44
PA (deg)	-36.48
$S_{1\text{cm}}$ (μJy)	128.8 ± 14.6
ν_{VLA} (GHz)	28.7–29.7
$T_{160\mu\text{m}-2\text{cm}}$ (K)	$20.4^{+0.5}_{-0.3}$
$S_{21\text{cm}}$ (μJy)	133.6 ± 25.3
$S_{850\mu\text{m}}$ (mJy)	24 ± 1
S_{ff} (μJy)	< 30.8
L_{bol} ($10^{13} L_{\odot}$)	0.69
L_{IR} ($10^{13} L_{\odot}$)	0.69
q_{IR}	> 3.00
χ^2	1.82

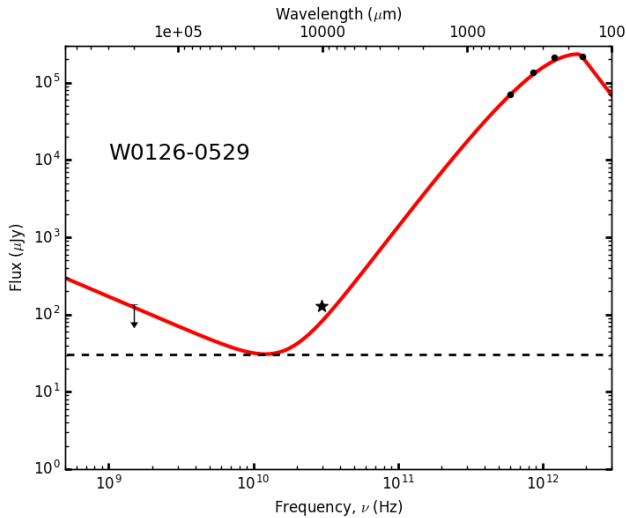


Figure A2. Observed frame SED for W0126-0529, using the same single temperature, modified blackbody fit to the $160\mu\text{m}$ to 2cm data with additional power-laws to fit for the remaining data. Radio data from FIRST and the VLA is fitted using a power-law ($S_{\nu} \propto \nu^{-0.8}$). The resultant curve is shown by a solid red line and a star has been used to denote the VLA data point. The dashed line indicates the maximum free-free emission possible.